Low-Frequency Meandering Piezoelectric Vibration Energy Harvester

David F. Berdy, *Student Member, IEEE*, Pornsak Srisungsitthisunti, Byunghoo Jung, *Member, IEEE*, Xianfan Xu, Jeffrey F. Rhoads, and Dimitrios Peroulis, *Member, IEEE*

***Abstract*—The design, fabrication, and characterization of a novel low-frequency meandering piezoelectric vibration energy harvester is presented. The energy harvester is designed for sensor node applications where the node targets a width-to-length aspect ratio close to 1:1 while simultaneously achieving a low resonant frequency. The measured power output and normalized power density are 118 μW and 5.02 μW/mm^3/g^2, respectively, when excited by an acceleration magnitude of 0.2 g at 49.7 Hz. The energy harvester consists of a laser-machined meandering PZT bimorph. Two methods, strain-matched electrode (SME) and strain-matched polarization (SMP), are utilized to mitigate the voltage cancellation caused by having both positive and negative strains in the piezoelectric layer during operation at the meander's first resonant frequency. We have performed finite element analysis and experimentally demonstrated a prototype harvester with a footprint of 27 × 23 mm and a height of 6.5 mm including the tip mass. The device achieves a low resonant frequency while maintaining a form factor suitable for sensor node applications. The meandering design enables energy harvesters to harvest energy from vibration sources with frequencies less than 100 Hz within a compact footprint.**

I. Introduction

In the past decade, piezoelectric vibration energy harvesting has been studied as a power source for wireless sensor nodes. Vibration energy harvesting is converting mechanical vibration energy into useful electrical energy by utilizing piezoelectric, electromagnetic, or electrostatic transducers. Several review articles on piezoelectric vibration energy harvesting are available in the literature [1]–[3]. The majority of the literature has focused on straight piezoelectric unimorph or bimorph cantilever beam energy harvesters [4]–[14], their optimization [8], and their modeling [6].

Energy harvesters are resonant devices and must be designed for a specific environment or application to optimally harvest power. Vibration studies show that most ambient vibration sources have peak vibration magnitude at low frequencies (less than 100 Hz) [15]–[17]. A spectral vibration study by Reilly *et al.* showed that 71% of the 21 ambient vibration sources characterized had peak vibration amplitudes below 100 Hz [15]. The low resonant frequency of vibration sources poses a problem in miniaturizing traditional piezoelectric cantilever harvesters because as energy harvester size is decreased, the resonant frequency tends to increase, which directly conflicts with the desire to achieve a low resonant frequency [16]. The main methods of decreasing resonant frequency are to increase the beam length or tip mass. However, if the application imposes constraints on length or tip mass, these methods may not be feasible.

Several experimentally demonstrated thick film piezoelectric energy harvesting devices from literature have resonant frequencies ranging from 26 to 120 Hz [4]–[8]. The low resonant frequencies are achieved by increasing the mass or length. The tip masses of the reported devices range from 9 to 167 g, whereas the lengths range from 28 to 96 mm. Using microfabrication, device thickness can be decreased to decrease the resonant frequency; however, microfabricated devices generally have relatively high resonant frequencies, for example, 277 and 870 Hz, as reported in [10] and [11]. Recently, two MEMS devices achieved sub-100 Hz resonant frequencies [13], [14]; however, these devices have normalized power densities orders of magnitude lower than bulk devices because of the poor piezoelectric properties of thin-film piezoelectrics common in MEMS energy harvesters.

A zig-zag energy harvester was presented recently to reduce the resonant frequency as compared with the typical straight cantilever energy harvester [18]–[20]. The zig-zag energy harvester is a fixed-free cantilever that has been turned around on itself to achieve a compact footprint while minimizing resonant frequency. In [19], it was shown that the resonant frequency of an 11-segment zig-zag is less than 1/17th that of a straight cantilever, showing great potential for reducing resonant frequency.

In this paper, we present a meandering piezoelectric vibration energy harvester designed to produce 100 μW power output while excited at 0.2 g (where 1 g is 9.8 m/s^2) peak acceleration at 50 Hz within a footprint of 27 × 23 mm, using a tip mass of only 1.92 g. The meandering design presented in this paper is a fixed-fixed design to reduce torsion at the anchor when compared to the fixed-fixed zig-zag design [18]–[20]. Additionally, full electromechanical experimental results of the energy harvester are presented, including harvested power. A preliminary implementation of the meander device was first presented

Manuscript received January 24, 2011; accepted January 31, 2012. The authors thank the Office of Naval Research for partial support under grant number N00014-09-1-0207 and the National Science Foundation for partial support under CAREER grant number 0747766.

D. F. Berdy and D. Peroulis are with the School of Electrical and Computer Engineering and the Birck Nanotechnology Center, Purdue University, West Lafayette, IN (e-mail: dberdy@purdue.edu).

P. Srisungsitthisunti, X. Xu, and J. Rhoads and are with the School of Mechanical Engineering and Birck Nanotechnology Center, Purdue University, West Lafayette, IN.

B. Jung is with the School of Electrical and Computer Engineering, Purdue University, West Lafayette, IN.

DOI http://dx.doi.org/10.1109/TUFFC.2012.2269

by the authors in [21]. The device in [21] consisted of a strain-matched electrode (SME) design to avoid voltage cancellation. In this paper, the device power output has been improved and a new strain-matched polarization (SMP) scheme is introduced to improve device robustness while avoiding voltage cancellation. Additionally, a more in-depth analysis is performed to predict device performance. The paper will present a qualitative analysis of the structure, provide finite element analysis (FEA) to predict performance, and experimental validation to verify the device operation.

The paper is organized as follows: Section II reviews the traditional cantilever piezoelectric vibration energy harvester approach. Section III discusses the operating principle of the low-frequency meandering design. Sections IV and V discuss the modeling, fabrication, experimental procedure, and results of two meander designs used to mitigate voltage cancellation and increase power output. Finally, a discussion of the results and conclusion from this work are provided in Sections VI and VII, respectively.

II. Traditional Vibration Energy Harvester

Typical piezoelectric vibration energy harvesters consist of a cantilevered piezoelectric bimorph beam as shown in Fig. 1. The fixed end of the beam is connected to a vibrating host structure and the free end of the beam has a tip mass attached to increase power output and tune the resonant frequency. The cross section consists of a center shim, two piezoelectric layers, and two electrode layers. The center shim is added to increase robustness and acts as an electrode depending on the polarization of the piezoelectric layers. The piezoelectric layers enable the conversion of mechanical energy into electrical energy via the piezoelectric effect. The electrode layers are thin layers of electrically conductive material deposited on the piezoelectric to collect the electric charge produced by the strained piezoelectric.

Piezoelectric materials produce an electric displacement when mechanically strained, or conversely a mechanical deformation when an electric field is applied. The constitutive equations for a piezoelectric material are described in [22]. For a differential element of piezoelectric material as shown in Fig. 1, with a uni-axial strain applied in the 1-direction, the electric displacement (D_3) is

$$D_3 = d_{31} S_1 Y_1 + \varepsilon_3^T \frac{V}{dZ}, \tag{1}$$

where d_{31} is the piezoelectric strain coefficient, S_1 is the applied 1-directed strain, Y_1 is the Young's modulus, ε_3^T is the permittivity at constant stress, V is the voltage across the differential element and dZ is the element's thickness [8]. The subscripts denote the axes, where the 3-axis is defined as the axis in the direction of polarization and, in this case, the 1-axis is the direction of the strain, as shown in Fig. 1. Assuming no voltage across the electrodes (i.e., short circuit), the charge (q_3) generated on the electrodes by the strained piezoelectric element is

$$q_3 = A D_3|_{V=0} = A d_{31} S_1 Y_1, \tag{2}$$

where A is the surface area of the differential piezoelectric element. Similarly, the open circuit voltage ($V_{3,\mathrm{oc}}$) of a strained piezoelectric element is found by setting D_3 to zero in [17]

$$V_{3,\mathrm{oc}} = -\frac{d_{31} dZ Y_1}{\varepsilon_3^T} S_1. \tag{3}$$

The cantilever beam energy harvester operates as follows. The host structure vibrates in the 3-direction, causing the beam to deflect in the 3-direction, inducing an alternating strain in the 1-direction as shown in the differential element. The alternating 1-directed strain, based on (2), produces an alternating charge on the electrodes. The actual charge produced on the beam electrodes requires integration over the entire piezo volume with the exact strain contour, but (2) shows the important result that the generated charge is proportional to strain. The current from the piezoelectric element through an attached electrical load is proportional to the time derivative of charge ($I = \mathrm{d}q/\mathrm{d}t$), and power is proportional to current squared; therefore, the power from the piezoelectric element is proportional to strain rate squared.

The mechanical resonant frequency of the energy harvester should be designed to closely match the driving frequency of the vibration source to maximize vibration-induced strain. Given that the power output is proportional to strain rate squared, the output power will be maximized at resonance [8]. The undamped natural frequency of a cantilever in transverse vibration is given by

$$\omega_\mathrm{n} = \sqrt{\frac{k_\mathrm{eq}}{m_\mathrm{eq}}} = \sqrt{\frac{3YI/L^3}{(33/140)mL + M_\mathrm{t}}}, \tag{4}$$

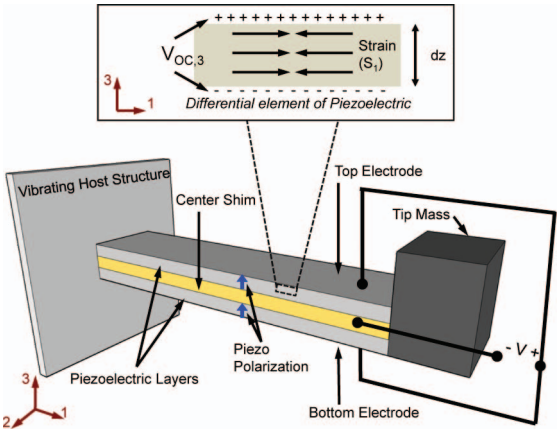

Fig. 1. Typical cantilever bimorph vibration energy harvester shown with parallel polarization of piezo layers.

where YI is the flexural rigidity of the beam, L is the length of the beam, m is the mass per unit length, and M_t is the tip mass [23]. The highest vibration amplitudes of typical vibration sources occur at low frequencies, below 100 Hz [15].

Based on (4), the resonant frequency can be decreased by decreasing the spring constant or increasing the mass. Some common methods of decreasing the resonant frequency include: 1) increasing the beam length, 2) increasing the tip mass, 3) decreasing the thickness (i.e., decreasing YI), and 4) decreasing the width (i.e., decreasing YI). Increasing the length or tip mass may be limited by the node size. It is possible to decrease the thickness to approximately 0.1 mm using bulk piezoelectric materials; however, microfabrication is required for further thickness reduction. Decreasing width or thickness while maintaining tip mass and length is a possibility, but maximum strain limitations must be considered. Additionally, decreasing the width of a beam while maintaining a constant length will make the footprint aspect ratio (length divided by width) of the energy harvester excessively large, which may not be desirable because electronics and sensor nodes generally have a rectangular shape with low aspect ratio. In this paper, we decrease the spring constant by utilizing a novel meandering structure, as shown in Fig. 2.

To more explicitly show that typical straight beam energy harvesters have difficulty meeting the low-frequency specification within the given space, three straight beam designs were simulated to compare their resonant frequencies and power output to the specified design goals. The design specification for this work is to achieve a resonant frequency of 50 Hz within a footprint of approximately 27 × 23 mm. The three beam designs, with the same material properties as the meander (discussed in Section IV), are:

- Long fixed-fixed beam: A 234-mm-long fixed-fixed beam with total length equal to the unfolded meander's length (Fig. 3).
- Wide fixed-fixed beam: A wide fixed-fixed beam with a footprint of 27 × 23 mm. The structure is similar to that shown in Fig. 4, except the tip mass is located at the center of the beam and the structure has fixed-fixed boundaries.
- Fixed-free beam: A wide fixed-free beam with a footprint of 27 × 23 mm and tip mass extending the entire width of the beam (Fig. 4).

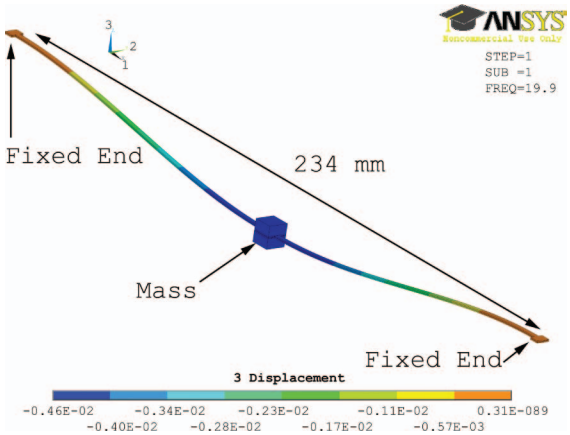

Fig. 3. First vibration mode (z-displacement) of a fixed-fixed beam of length equal to the unfolded meander length.

The three straight-beam simulation results are compared with the desired specifications in Table I. The long fixed-fixed beam achieves a low resonant frequency of 19.9 Hz; however, it has an excessively long length of 234 mm, which makes it unsuitable for most applications. Additionally, the long fixed-fixed beam exceeds the maximum strain limit of 500 μstrain by 40% (700 μstrain). The other two beams, wide fixed-fixed and wide fixed-free, have resonant frequencies of 1648 and 175 Hz, respectively, which are much higher than the desired resonant frequency of 50 Hz. In the remainder of the paper, the meandering energy harvester will be introduced, discussed in detail, and shown to meet the desired specifications.

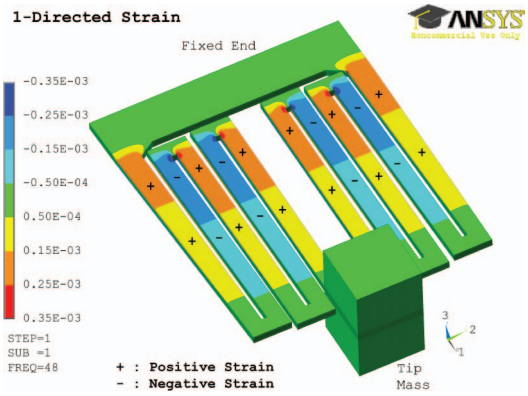

Fig. 2. Simulated 1-directed strain contour of the proposed meandering energy harvester, showing positive and negative strain locations along the top piezoelectric layer surface.

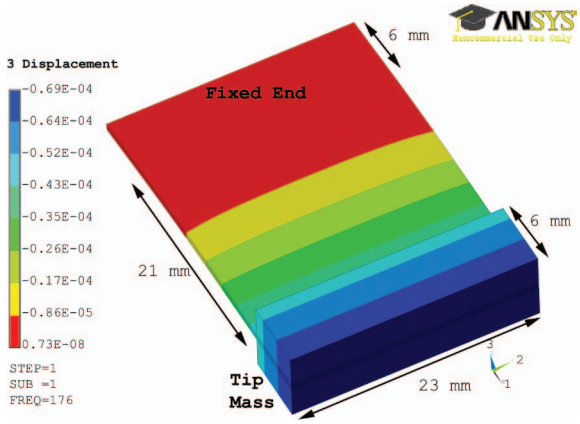

Fig. 4. First vibration mode (z-displacement) of a wide fixed-free cantilever.

TABLE I. BEAM SIMULATION RESULTS.

Design	Footprint (mm)	Tip mass (g)	f_n (Hz)	Power (sim.) (μW)
Desired specification	27 × 23	1.92	50	100
Meander (SMP)	27 × 23	1.92	49.7	130
Long fixed-fixed beam	234 × 1.5	1.92	19.9	310*
Wide fixed-fixed beam	27 × 23	6.55	1648	10.2*
Wide fixed-free beam	27 × 23	6.55	175	89.8

*Used two electrodes to avoid voltage cancellation.
The meander strain-matched polarization (SMP) design is introduced in Section V.

III. MEANDERING ENERGY HARVESTER

A. Meandering Harvester

Reduction of the mechanical resonant frequency is achieved in this work by a meandering piezoelectric vibration energy harvester design. To the author's knowledge, this is the first time a meandering structure has been experimentally demonstrated in piezoelectric vibration energy harvesting. Meandering structures are commonly used in antenna design to reduce antenna size [24] and in MEMS switches to decrease the actuation voltage by reducing the spring constant [25]. Additionally, piezoelectric meanders have been implemented to achieve large displacements with relatively low actuation voltages in micropositioners [26] and micromirrors [27].

The proposed meandering energy harvester is shown in Figs. 2 and 5. Essentially, the meander is a long straight fixed-fixed beam which has been bent to reduce the maximum dimension (i.e., length) of the harvester. The meander structure reduces the spring constant when compared with a similar length fixed-fixed beam. The reduction in spring constant leads to a lower resonant frequency, and the meandering reduces the maximum dimension compared with a straight beam. The meander uses the same bimorph material cross section as the straight cantilever shown in Fig. 1. A tip mass is attached to increase power output and tune the resonant frequency.

The meandering structure is a fixed-fixed structure. Fixed-fixed structures typically have higher resonant frequencies than similar fixed-free structures; however, simulations showed that utilizing a fixed-free structure with only one half of the meander structure (i.e., above the dashed line in Fig. 5) resulted in approximately 1.3× higher shear strain at the anchor points and connections between meander segments. The higher shear strain can cause fracture in the electrode and piezoelectric material, leading to failure. Therefore a fixed-fixed structure was chosen to reduce torsion at the anchor and increase overall robustness.

B. Meander Voltage Cancellation

A problem of voltage cancellation potentially reduces power output in piezoelectric energy harvesters. Based on the definition of a piezoelectric material, as seen specifically in (3), the voltage produced on the electrodes of a piezoelectric material is proportional to the strain in the piezoelectric layer. Therefore, if an element of piezoelectric material has a positive strain (tension) in one location and a negative strain (compression) in another location, negative and positive voltages will be produced across the piezoelectric material. If a continuous electrode covers the entire piezoelectric layer, the negative and positive voltages will tend to cancel. This concept was presented in [28] for a straight cantilever beam, in which the term *strain node* was defined as the location on the beam where the bending strain distribution changes sign for a vibration mode. Therefore, to avoid voltage cancellation, the idea of cutting the electrode at strain nodes was introduced [28], and is referred to as SME in this paper.

The meander has a first resonant mode shape with both positive and negative strains present in the piezoelectric layers, resulting in voltage cancellation. Consider a two-beam meander section with tip mass, as shown in Fig. 6. During resonant operation, the motion of the tip mass causes beam 2 to bend down. This leads to a torque on the section connecting beam 1 to beam 2. This torque is transferred to the end of beam 1. The other boundary of beam 1 is vibrating with relatively small amplitude, and is essentially fixed. The torque is transferred from beam 2 to beam 1, causing beam 1 to bend up. Based on this qualitative analysis, beam 1 and beam 2 have opposite curvatures. The opposite curvatures result in opposite strains in the piezoelectric layers of beam 1 and beam 2, therefore resulting in voltage cancellation if a single electrode covers the piezo layers of both beams, based on (3).

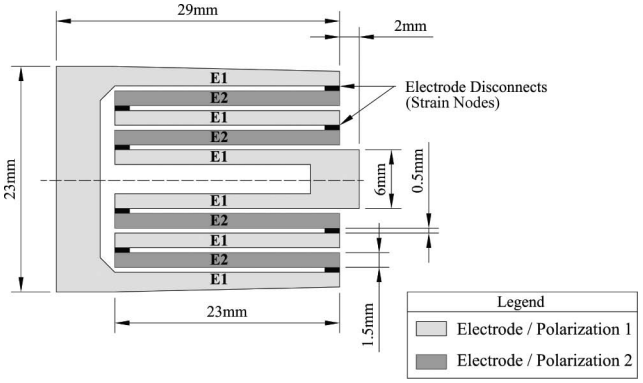

Fig. 5. Top view of meandering piezoelectric vibration energy harvester with dimensions, strain-matched electrodes, and strain-matched polarizations shown.

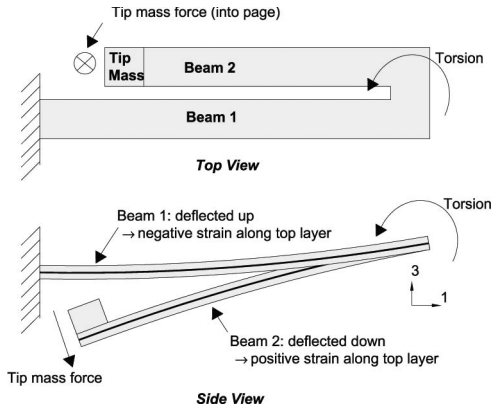

Fig. 6. Top and side views of a two-beam meander at peak amplitude showing positive and negative strains in the top piezoelectric layer.

This analysis of the contour in a simplified two-beam meander can be extended to the meander shown in Fig. 2. To verify this intuitive conclusion, the meander was simulated and the strain contour was plotted as shown in Fig. 2. The strain along the top electrode–piezoelectric interface shows both positive (+) and negative (−) strain components, leading to both negative and positive voltages. If we assume that only a single electrode is deposited on the piezoelectric layer, the positive and negative voltages will cancel, significantly reducing the power output. We call this the single-electrode device.

The voltage cancellation issue was resolved in this work by two methods: SME and SMP. The basic idea is to separate the positive and negative strain regions. The modeling, fabrication and experimental results will be given for both devices in the following sections.

IV. Design 1: Strain-Matched Electrode

In the SME technique, two electrodes are used to separately harvest energy from the positive and negative strain regions. The electrodes of the SME design are shown in Fig. 5. Electrode E1 covers the piezoelectric material at strain locations of one polarity (i.e., strain > 0) whereas electrode E2 covers strain locations of the opposite polarity (i.e., strain < 0). The two electrodes are electrically isolated at strain nodes to avoid cancellation of negative and positive voltages.

A. Modeling and Simulation

Full analytic modeling of the meandering energy harvester is beyond the scope of this paper. The approach we take to model the energy harvester and predict its performance is to reduce the model to a single mode lumped-element, spring-mass-dashpot system with piezoelectric coupling included. The power output from the device can then be determined from the overall system parameters [16]. The system parameters are determined by finite element analysis (FEA) in this work. The system parameters used to calculate the harvested power include base acceleration amplitude ($A_{(\mathrm{peak})}$), effective mass (m_{eq}), natural frequency (ω_{n}), normalized frequency (Ω), normalized resistance (r), damping ratio (ζ), and electromechanical coupling (k_{e}).

The acceleration is determined by the particular application and operating environment; in our application, it has an amplitude of 0.2 g at 50 Hz. The equivalent mass (m_{eq}) can be found by solving (4) for m_{eq} using the spring constant and natural frequency, or by extracting it from the FEA results. The natural frequency (f_{n}) is found using a modal analysis in the FEA simulation. The operating frequency is assumed to match the natural frequency ($\Omega = 1$) and the resistance can vary, although there is an optimal resistive load at $r = 1$. The only system parameter that cannot be determined through simulation is the mechanical damping factor (ζ), which must be determined experimentally.

The electromechanical coupling coefficient (k_{e}) is an important system parameter for piezoelectric energy harvesters [17]. The electromechanical coupling is a measure of a material or system's ability to convert mechanical energy into electrical energy or vice versa. In energy harvesting, k_{e} is ideally maximized, leading to a high conversion of mechanical energy into electrical energy. Values of k_{e} for different piezoelectric materials range from 0.11 to 0.91 [17]; however, the system's coupling coefficient is usually lower than the piezo material's coupling coefficient because of the use of structural materials. The system coupling coefficient of a device can be found by

$$k_{\mathrm{e}}^2 = \frac{f_{\mathrm{oc}}^2 - f_{\mathrm{sc}}^2}{f_{\mathrm{oc}}^2}, \tag{5}$$

where f_{oc} and f_{sc} are the open-circuit and short-circuit resonant frequencies [8]. The electromechanical coupling coefficient was found in simulation by performing a modal analysis of the meander in the open-circuit and short-circuit (i.e., all electrodes shorted together) configurations to determine the resonant frequencies.

Using the system parameters, the rms ac power output can be calculated from

$$P_{\mathrm{ac,rms}} = \frac{1}{2}\frac{\left(m_{\mathrm{eq}}A_{(\mathrm{peak})}\right)^2}{\omega_{\mathrm{n}}m_{\mathrm{eq}}} \times \frac{rk_{\mathrm{e}}^2\Omega^2}{[1-(1+2\zeta r)\Omega^2]^2 + [(1+k_{\mathrm{e}}^2)r\Omega + 2\zeta\Omega - r\Omega^3]^2}, \tag{6}$$

which is derived from a single mode spring-mass-dashpot model with piezoelectric coupling included. The derivations and details of (6) can be found in [16].

The finite element modeling package Ansys 11.0 (Ansys Inc., Canonsburg, PA) was used to determine the energy harvester system parameters. The center shim and tip mass were modeled using Ansys element SOLID45 and the piezoelectric was modeled using element SOLID5. All nodes of the center shim were set to a voltage of zero to

specify it as the reference electrode. The electrodes on the piezoelectric surface were modeled by selectively coupling the VOLT degree-of-freedom. The SME design selectively coupled the voltages of specific meander beam sections to achieve the electrode configuration seen in Fig. 5.

The nodes attached to the vibrating host structure were excited at the desired acceleration amplitude with a harmonic-imposed displacement as determined from

$$|Y| = \frac{A_{(\text{peak})}}{(2\pi f)^2}, \tag{7}$$

where Y is the imposed base displacement amplitude, $A_{(\text{peak})}$ is the peak acceleration amplitude and f is the first mode resonant frequency [29].

The model was analyzed using a harmonic analysis to find the strains and voltages produced across the electrodes as shown in Figs. 2 and 7. The strain shows both positive and negative values, as discussed previously, leading to both positive and negative voltages. The single-electrode device has an open-circuit voltage amplitude of 1.62 V. On the other hand, the SME design has an open circuit voltage of −6.57 and 9.29 V for electrodes E1 and E2, respectively. The SME design has higher voltage than the single electrode design because of the avoidance of voltage cancellation.

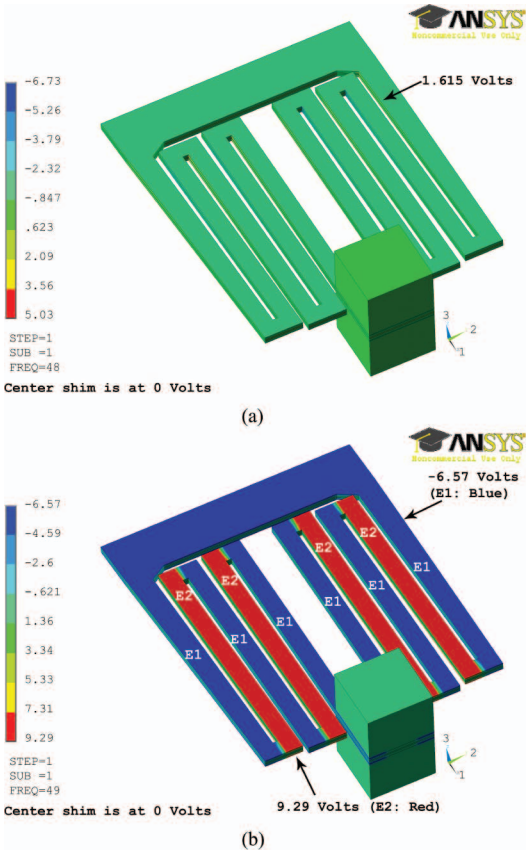

Fig. 7. Simulated open-circuit voltages (as referenced to the center shim electrode) for (a) single-electrode and (b) strain-matched electrode designs.

A brief comparison of the relative charge produced by each device can be obtained by looking at the peak charge stored by the device. The charge stored in the piezoelectric capacitance can be calculated as

$$Q_{\text{cap}} = CV, \tag{8}$$

where C is the capacitance between electrodes, V is the voltage produced, and Q_{cap} is the total charge produced by the harvester at peak displacement. The capacitance of the single-electrode design is 58.7 nF, whereas the SME has capacitances of 37.4 and 16.3 nF for E1 and E2, respectively. Based on the voltage and capacitance values, the charge stored in the piezoelectric capacitor at the peak displacement is 94.8 and 397 nC (246 nC + 151 nC) for the single-electrode and SME designs, respectively. The charge analysis clearly shows that the SME design produces more charge than the single-electrode design, giving an approximate comparison of the two configurations.

The simulated system parameters of the single electrode and SME meandering harvesters are shown in Table II. Because of voltage cancellation, the single electrode design is expected to have a much lower coupling coefficient (k_e), which is evidenced by the 0.045 and 0.23 coupling coefficients of the single-electrode and SME designs, respectively. Therefore, the SME design has a much higher power output. Based on the simulated system parameters, the estimated power outputs are 14 and 120 μW for the single-electrode and SME designs, respectively.

B. Fabrication

The piezoelectric material used to fabricate the device consists of a parallel-poled bimorph (T226-A4–503Y, Piezo Systems Inc., Woburn, MA). The material has a cross section as shown in Fig. 1, consisting of two 0.27-mm-thick industry-type 5A lead zirconate titanate (PZT) piezoelectric layers, a 0.13-mm-thick center brass layer, and thin nickel electrodes. Table III shows the material properties and other model parameters. The acceleration magnitude of 1.96 m/s^2 is a typical value for many ambient vibrations, for example, a Lenovo laptop or a heating, ventilation, and air conditioning (HVAC) vent [15].

The meandering piezoelectric energy harvesters were fabricated by laser-machining the bimorph material using a femtosecond pulsed laser. The material moved on a

TABLE II. ENERGY HARVESTER SYSTEM PARAMETERS.

Parameter	Single electrode	SME	SMP
$A_{(\text{peak})}$ (m/s^2)	1.96	1.96	1.96
m_{eq} (g)	2.8	2.8	2.8
f_{n} (Hz)	48	49	49
$\Omega = f/f_{\text{n}}$	1	1	1
r	1	1	1
ζ	0.018	0.018	0.016
k_{e}	0.045	0.23	0.21
$P_{\text{ac,max}}$ (μW)	14	120	130

SME = strain-matched electrode; SMP = strain-matched polarization.

high-precision three-axis motion stage controlled by custom CAD-CAM software. The meander is shown in Fig. 8, after completion of laser machining. Electrical isolation of the electrodes was accomplished by brazing the electrode at the electrode disconnect locations.

In the SME design, the separate segments of electrode E1 were electrically connected using thin wires soldered to the electrodes between meander sections, as seen in Fig. 9. Electrode E2 was connected similarly. After the electrode connections were made, the device was attached to an FR4 mount with cyanoacrylate. Wires were soldered to the electrodes to make electrical connections to the device. Three wires were attached: one for the brass shim (i.e., reference electrode), one for electrode E1, and one for electrode E2. The center brass was accessed by removing a portion of the top layer of piezoelectric material. The wires were bonded to the FR4 to hold the wires in place during mechanical excitation.

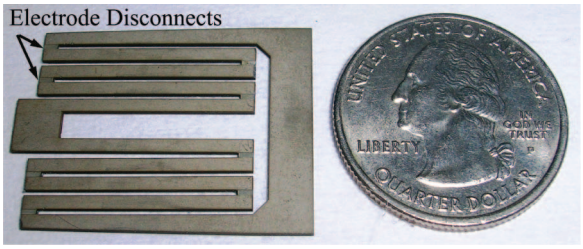

Fig. 8. Laser-machined meandering piezoelectric energy harvester. A US quarter is shown for scale.

C. Experimental Results

The fabricated devices were tested to validate the modeling results. Voltage was measured with an oscilloscope with 1 MΩ input resistance and a 10:1 probe. As a result, any load resistor connected to the circuit was adjusted to account for the input resistance of 10 MΩ. The imposed displacement vibration was applied with an electrodynamic shaker (TV 51120, TIRA GmbH, Schalkau, Germany). The acceleration of the imposed displacement was measured with a single-axis MEMS accelerometer (CXL-04GP1Z, Crossbow Technology Inc., San Jose, CA). The meandering energy harvester attached to the FR4 was mounted on the vibration shaker with screws, as shown in Fig. 9.

The SME design has three electrodes: E1, E2, and the center shim electrode, each at a different voltage in the open-circuit condition, as shown schematically using a simplified piezoelectric model in Fig. 10. The highest voltage difference is seen from electrode E1 to E2, therefore the electrical load should be connected across these electrodes. Connecting the load from E1 to E2 means that the piezoelectric layers under E1 are electrically in series with the piezoelectric layers under E2. If E1 and E2 are electrically connected together, the SME acts as a single-electrode meander because the positive and negative strain electrodes are shorted, resulting in voltage cancellation. The single-electrode meander was measured in this way.

The open-circuit and short-circuit resonant frequencies were measured to determine the system coupling coefficient from (5). The open-circuit resonant frequency was determined by sweeping the shaker excitation frequency to find the frequency which produced the highest voltage amplitude. The short-circuit resonant frequency was measured by connecting the energy harvester directly to a 1 kΩ load, or less than 1/50 the optimal load, to approach the short-circuit condition, and sweeping the frequency again to maximize the voltage. A sweep of the open-circuit output voltage versus frequency is shown in Fig. 11. The measured open-circuit and short-circuit resonant frequencies of the SME design were 49.8 and 48.9 Hz, respectively. The measured resonant frequencies are within 3% of the simulated values. The deviation in resonant frequency can be explained by differences in material properties and fabrication tolerance. Another point to note from Fig. 11 is that the frequency response curve shows some small asymmetry. This asymmetry is potentially a result of

TABLE III. MATERIAL AND SIMULATION PROPERTIES.

Piezoelectric properties	
Relative dielectric constant (ε_r)	1800
33 Piezoelectric strain coefficient (d_{33})	390×10^{-12} m/V
31 Piezoelectric strain coefficient (d_{31})	-190×10^{-12} m/V
Piezoelectric density ρ_p	7800 kg/m^3
Elastic modulus (Y_3^E)	5.2×10^{10} N/m^2
Elastic modulus (Y_1^E)	6.6×10^{10} N/m^2
Piezo thickness (t_p)	0.27 mm
Shim and tip mass properties	
Shim density (ρ_s)	8500 kg/m^3
Shim elastic modulus (E_s)	10×10^{10} N/m^2
Center shim thickness(t_s)	0.13 mm
Tip mass density (ρ_{tm})	7400 kg/m^3
Other parameters	
Acceleration magnitude ($A_{(peak)}$)	1.96 m/s^2
Device volume	588 mm^3
Tip mass	1.92 g
Total device mass	4.4 g

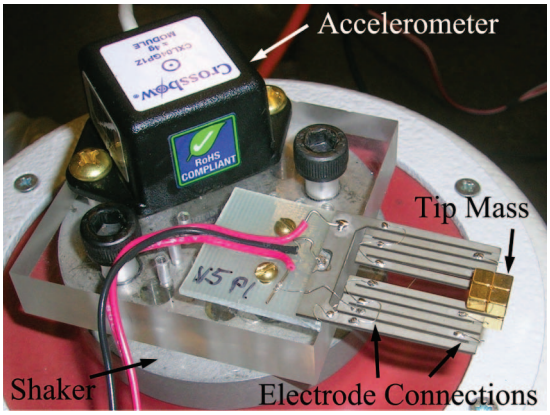

Fig. 9. Strain-matched electrode meandering energy harvester mounted on electrodynamic shaker for testing.

some form of nonlinearity in the device, however, further study is required to determine its exact source.

The open-circuit and short-circuit resonant frequencies are used to calculate the coupling coefficient as in (5). The SME measured coupling coefficient is 0.19. Table IV compares the simulated and measured electromechanical coupling. The measured coupling coefficient is lower than the simulated value. The difference between the measured and simulated coupling coefficients is explained by the lack of modeling of the bonding layers and material property variation.

The mechanical damping ratio (ζ) of the structure was determined from a ring-down test by exciting the energy harvester at its resonant frequency and abruptly stopping the shaker to view the ringdown waveform. The damping ratio was calculated from the ring-down waveform based on the equation

$$\zeta = \frac{1}{2\pi n} \ln\left(\frac{x_1}{x_n}\right), \tag{9}$$

where x_1 is the voltage magnitude at one peak of the oscillation and x_n is the peak voltage n periods later [17]. The SME's measured damping ratio was calculated as 0.018 by averaging 10 measurements, which had a standard deviation of 0.0018. The damping ratio heavily influences the open-circuit voltage amplitude and, therefore, power output. Comparing the finite-element-simulated peak open-circuit voltage and the measured open-circuit voltage in Table IV, which deviate by less than 5%, it is concluded that the ring-down test gives a good estimate of the mechanical damping ratio.

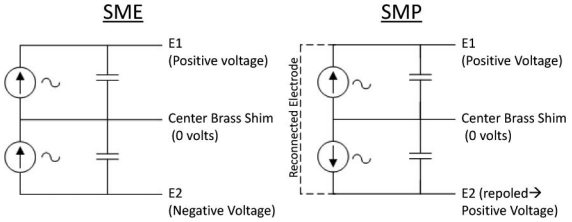

Fig. 10. Schematic showing voltage polarity of strain-matched electrode (SME) and strain-matched polarization (SMP) designs with simplified piezoelectric model.

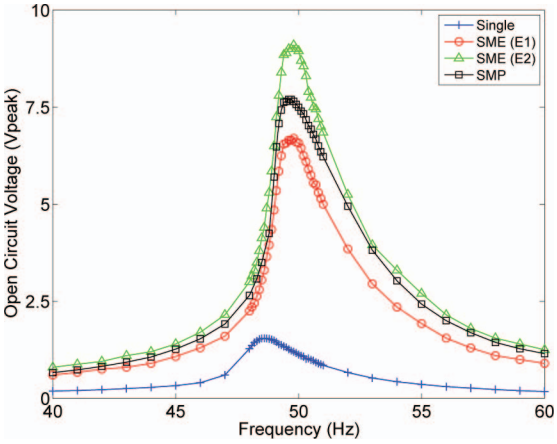

Fig. 11. Measured open-circuit voltage of meandered piezoelectric energy harvester versus frequency.

The ac rms power output was measured by connecting the energy harvester directly to a load resistor. The resistance was swept to find the optimal load. Power output as a function of resistance is shown in Fig. 12. The SME design achieved optimal power output of 105 μW at a load resistance of 380 kΩ. The dc power output was also measured by connecting the harvester to a diode bridge rectifier consisting of 4 BAT46 diodes (ST Microelectronics, Geneva, Switzerland) and a 3.3-μF filter capacitor. The dc power at the optimal load of 600 kΩ was 84 μW. The simulated power output using the spring-mass-dashpot model and finite element simulation results is higher than the measured power output because the measured coupling coefficient is lower than the simulated value, as seen in Table IV. If the measured k_e is substituted into the spring-mass-dashpot power equations, the calculated optimal power is close to the measured optimal power.

Two figures of merit to compare energy harvesters are power density (PD) and normalized power density (NPD). The power density is the power per device volume, and the NPD is defined as the power density per acceleration squared. The power density and normalized power density for the SME design are 0.18 μW/mm^3 and 4.46 μW/mm^3/g^2, respectively. Thick-film bulk-PZT devices reported in the literature have NPDs ranging from 0.004 to 6.8 μW/mm^3/g^2 [4]–[6], [8].

The single-electrode device was measured using the SME design with electrodes E1 and E2 electrically connected together. The single-electrode design open- and short-circuit resonant frequencies were too close to be experimentally observed, therefore the coupling is very low. The measured damping was 0.018. The measured open-circuit voltage amplitude was 1.55 V. The maximum ac rms power output of the single-electrode design operating at its resonant frequency of 48.6 Hz was 5.5 μW at a load resistance of 60 kΩ. The dc power was measured as 5.0 μW at 60 kΩ. As expected, the power output of the single-electrode device is well below that of the SME design because of voltage cancellation.

TABLE IV. SIMULATION (SIM.) AND MEASUREMENT (MEAS.) RESULTS.

	Single electrode		SME		SMP	
	Sim.	Meas.	Sim.	Meas.	Sim.	Meas.
f_{sc} (Hz)	47.94	—	47.7	48.9	47.9	48.9
f_{oc} (Hz)	48.0	48.6	49.0	49.8	49.0	49.7
k_e	0.045	—	0.23	0.19	0.21	0.18
$V_{oc(peak)}$ (V)	1.6	1.6	15.9	15.8	8.1	7.7
ζ	—	0.018	—	0.018	—	0.016
$P_{ac,rms}$ (μW)	14	5.5	120	105	130	118
R_{opt} ($k\Omega$)	50	60	500	380	90	60
P_{ac}/vol. (μW/mm^3)	0.026	0.009	0.213	0.18	0.238	0.20
NPD (μW/mm^3·g^2)	0.64	0.225	5.23	4.46	5.94	5.02
P_{dc} (μW)	—	5	—	84	—	93

SME = strain-matched electrode; SMP = strain-matched polarization; NPD = normalized power density.

V. DESIGN 2: STRAIN-MATCHED POLARIZATION

In the SMP technique, the piezoelectric material is re-poled such that the piezoelectric layers under E2 have a polarization opposite that of the material under E1. This repolarization is shown schematically in Fig. 10. The SMP approach effectively inverts the voltage polarity of one of the electrodes of the SME design so that in the first vibration mode, the electrodes will have the same voltage polarity. Having the same voltage polarity on E1 and E2 allows E1 and E2 to be connected together, as shown in Fig. 10, connecting their piezoelectric layers electrically in parallel. The SMP scheme uses a single continuous electrode across the entire piezoelectric, and therefore does not require complicated wiring between electrodes as the SME design does.

A. Modeling and Simulation

The SMP used the same modeling and simulation procedure discussed for the SME design. The re-poled piezoelectric was modeled in Ansys using two relative coordinate systems, one with the 3-axis (or polarization direction) in the positive z-direction to represent polarization of the piezoelectric material under electrode E1 and the other in the negative z-direction to model the opposite polarization of piezoelectric material under electrode E2. The simulated open-circuit device voltage is shown in Fig. 13. The simulation results for the SMP are listed in Table IV. The simulated optimal power output is 130 μW, slightly higher than the SME simulated power output because of the lower experimentally observed damping.

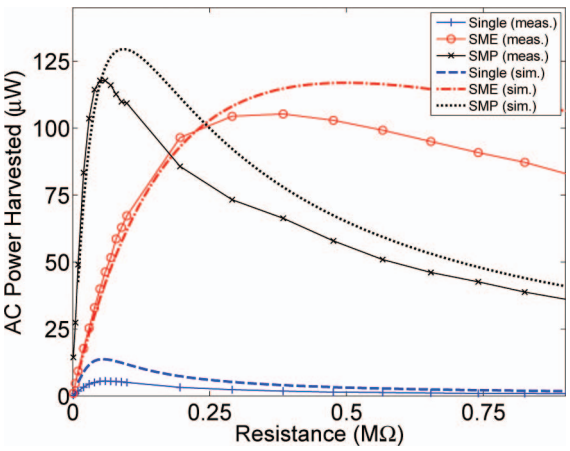

Fig. 12. Measured and simulated ac power of meandered piezoelectric energy harvester versus resistance for single-electrode, strain-matched electrode (SME), and strain-matched polarization (SMP) designs.

B. Fabrication

The SMP design was laser-machined in the same way as the SME design, with the electrode disconnections as shown in Fig. 8. To selectively re-pole the piezoelectric material, the device was sandwiched between two printed circuit boards (PCBs) fabricated to connect an external supply to specific electrodes of the meandering device. An electric field of 2600 V/mm (700 V across 0.27 mm) was applied between the center brass shim and the outer electrode for a duration of 45 min to re-polarize the piezoelectric material. The value of 2600 V/mm is based on the 50 to 100 V/mil (2000 to 4000 V/mm) recommended by the material manufacturer to re-pole the material. After repoling, the electrode was repaired at the electrode disconnects with a silver conductive pen to form a single electrode covering the piezoelectric layer. Fig. 14 shows the fabricated SMP meandering energy harvester mounted for testing on the electrodynamic shaker.

C. Experimental Results

The SMP design was measured using the same procedure as the single-electrode and SME designs. The results are summarized in Table IV. The measured open-circuit and short-circuit resonant frequencies were 49.7 and 48.9 Hz, respectively, resulting in a coupling coefficient of 0.18. The measured damping was 0.016, which is lower than the 0.018 damping of the SME design. The higher damping of the SME is potentially due to the soldered wires connecting the electrode segments and variations in fabrication. The measured open-circuit voltage amplitude was 7.7 V. The maximum ac rms power output of the SMP design operating at its open-circuit resonant fre-

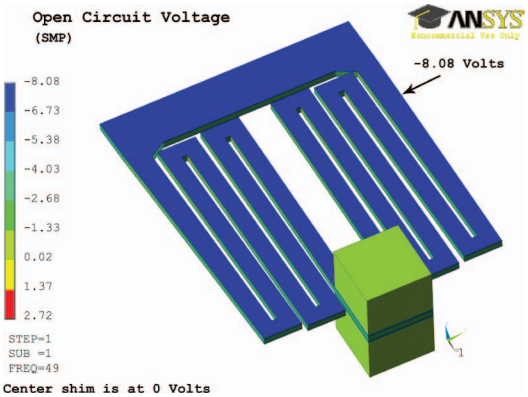

Fig. 13. Simulated open-circuit voltage (as referenced to center shim) for the meandering strain-matched polarization (SMP) design.

quency was 118 μW at a load resistance of 60 kΩ. The dc output power was measured to be 93 μW at a load of 150 kΩ. The SMP design achieves a slightly higher power output than the SME design because of its lower damping.

The SME and SMP show different optimal load resistances, although they have the same dimensions and tip mass. The measured power output is a function of load resistance as shown in Fig. 12 for the single-electrode, SME, and SMP designs. The optimal load depends on many factors, but here we focus on the configuration of the piezoelectric material. In the SME design, the piezoelectric layers under electrode E1 and E2 are connected in series as shown in Fig. 10, resulting in the addition of their voltages. The SMP design, with one electrode repoled, has the piezoelectric layers all connected in parallel, which results in a higher current rather than higher voltage compared with the SME design. Based on Ohm's law, the higher voltage of the SME design results in a larger source impedance, requiring a larger load resistance to match this impedance.

In summary, by utilizing the meander-shaped energy harvester, the single-electrode, SME, and SMP designs have their own advantages and disadvantages. A low resonant frequency of 50 Hz within a compact space is the key advantage of all three devices. The single-electrode device shows the lowest performance as a result of voltage cancellation, however manufacturing is the least complex because a single continuous electrode can be used. The SME and SMP designs achieve a significantly higher power output (about 20× higher) compared with the single-electrode device because of avoidance of voltage cancellation, but at the expense of increased manufacturing complexity. The SME design requires the separate electrode segments of electrode E1 and E2 to be connected with thin wires soldered between segments, which potentially reduces device robustness and increases manufacturing complexity. The SMP design removes the need for connecting separate electrode segments; however, the repolarization of specific piezoelectric segments adds manufacturing complexity. Of the three designs, the SMP is the most robust device, with the highest performance.

VI. Discussion

A sample of energy harvesters from literature, using PZT, lead magnesium niobate-lead titanate (PMN-PT), AlN, and MEMS fabrication techniques (M), are listed in Table V. The most common energy harvester figures of merit stated in literature are PD and NPD. NPD gives a fairer comparison across applications, because it takes into account the acceleration amplitude. The meandering energy harvester has an NPD of 5 $\mu W/mm^3/g^2$, which is comparable to other bulk PZT devices with NPD ranging from 0.004 to 6.8 $\mu W/mm^3/g^2$. The NPD of the device in [7] is much higher than the rest because the device uses PMN-PT, which has significantly higher piezoelectric constants.

The natural frequencies of the devices in Table V range from 26.375 Hz to 13.9 kHz because of their various dimensions and material properties. Ideally, in energy harvesting, we would like to minimize device resonant frequency, while also minimizing the volume. A new figure of merit, called the frequency figure of merit (f_{FOM}) is introduced here to compare various energy harvesters of different sizes. The f_{FOM} metric is defined as the product of frequency and device volume; low values are desired. Comparing the meandering device to the bulk devices in [4]–[8], the meander has the lowest f_{FOM} of 29.2 $cm^3{\cdot}Hz$. The MEMS fabricated devices in [9]–[12] all have resonant frequencies higher than 190 Hz, which is too high for most ambient vibration sources. However they are capable of achieving a low f_{FOM}, as low as 0.228 $cm^3{\cdot}Hz$. The reason for the lower f_{FOM} of the MEMS devices is that by utilizing micromachining techniques, the thickness of the beam can be significantly reduced, achieving a length-to-thickness ratio of up to 1000:1. The MEMS devices in [13] and [14] do achieve low resonant frequencies of 47 and 85.5 Hz, respectively, because of their high length-to-thickness ratio; however, their power output and normalized power density are several orders of magnitude lower than the

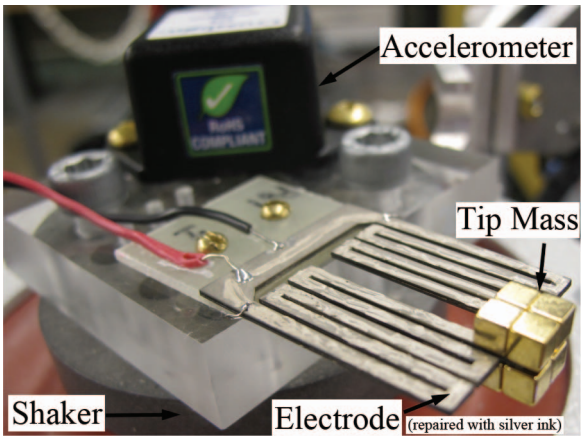

Fig. 14. Strain-matched polarization (SMP) meandering energy harvester mounted on electrodynamic shaker for testing.

TABLE V. ENERGY HARVESTER MEASUREMENT RESULTS FROM THE LITERATURE.

RMS power (μW)	Frequency (Hz)	Accel. (g_{peak})	Vol. (mm^3)	f_{FOM} (cm^3·Hz)	Tip mass (g)	PD (μW/mm^3)	NPD (μW/mm^3·g^2)	Method	Reference
118	49.7	0.2	588	29.2	1.92	0.20	5.02	PZT	This work
86	26.375	0.17*	21 280	561	153	0.004	0.14	PZT	[4]
29.3	27	0.05	3106	83.9	52	0.009	3.77	PZT	[5]
23 900	45.6	1	3520	160	12	6.8	6.8	PZT	[6]
19 000	60	0.2	26 240	1574	167	0.72	18.1	PMN-PT	[7]
375	120	0.25	1000	120	9	0.375	6	PZT	[8]
65	190	7.1	1.2	0.228	0	54.2	1.07	PMN-PT (M)	[9]
32.2	277	1	31*	8.59	0.07	1.04	1.04	AlN (M)	[10]
0.565*	870	8	3.75	3.26	0.003	0.150	0.0024	PZT (M)	[11]
1	13 900	10.6*	0.027	0.375	N/A	37.04	0.33	PZT (M)	[12]
0.0855	47	1	10.1	0.475	0.023	0.0085	0.0085	PZT (M)	[13]
0.00029	85.8	0.166	3.43*	0.294	0.008*	8.45×10^{-5}	0.0031	PZT (M)	[14]

*Values have been interpolated from data given in the referenced literature.
PD = power density; NPD = normalized power density; PZT = lead zirconate titanate; PMN-PT = lead magnesium niobate-lead titanate; (M) = MEMS-fabricated.

bulk thick film devices because of the fabrication difficulties in making high-quality thin-film piezoelectric layers.

An additional advantage of the meander design not discussed in this paper is the potential for wideband energy harvesting. The meander's close natural frequency spacing can be exploited to achieve a large bandwidth [30]. Future work will focus on further exploration of using the meander for bandwidth enhancement.

VII. CONCLUSION

In this paper, the design, simulation, and experimental results of a compact, low-frequency, piezoelectric vibration energy harvesting device were presented. The meander-shaped piezoelectric energy harvester effectively achieves a lower resonant frequency compared with a straight cantilever-beam harvester of similar length, allowing effective harvesting from low-frequency vibrations. The meander design is especially promising for reducing resonant frequencies in MEMS energy harvesters, which have been suggested to have a lower resonant frequency limit of 100 Hz [31]. Voltage cancellation in the meander design was mitigated by using the SME and SMP designs, improving the power output by over 10× compared with the single-electrode meander device. The meander achieves an NPD of 5.02 μW/mm^3/g^2, which is comparable to previously reported devices in literature. The ac and dc power output from the device under typical ambient vibrations (0.2 g at 49 Hz) were measured to be 118 and 93 μW, respectively, potentially enough to power a low-power, low-duty-cycle wireless sensor node system. Future studies of the meandering design should include analytic modeling, device optimization, MEMS fabrication, and integration with an entire sensor node.

REFERENCES

[1] H. A. Sodano, D. J. Inman, and G. Park, "A review of power harvesting from vibration using piezoelectric materials," *Shock Vib. Dig.*, vol. 36, no. 3, pp. 197–205, May 2004.

[2] S. R. Anton and H. A. Sodano, "A review of power harvesting using piezoelectric materials (2003–2006)," *Smart Mater. Struct.*, vol. 16, no. 3, pp. R1–R21, Jun. 2007.

[3] H.-U. Kim, W.-H. Lee, H. V. R. Dias, and S. Priya, "Piezoelectric microgenerators—Current status and challenges," *IEEE Trans. Ultrason. Ferroelectr. Freq. Control*, vol. 56, no. 8, pp. 1555–1568, Aug. 2009.

[4] K. Adachi and T. Tanaka, "An experimental power generation evaluation of cantilever type of piezoelectric vibration energy harvester," in *ASME Conf. Smart Materials, Adaptive Structures and Intelligent Systems*, 2009, pp. 281–289.

[5] E. S. Leland, E. M. Lai, and P. K. Wright, "A self-powered wireless sensor for indoor environmental monitoring," in *Wireless Networking Symp.*, 2004, pp. 1–5.

[6] A. Erturk and D. J. Inman, "An experimentally validated bimorph cantilever model for piezoelectric energy harvesting from base excitations," *Smart Mater. Struct.*, vol. 18, no. 2, art. no. 025009, 2009.

[7] H. J. Song, Y. T. Choi, G. Wang, and N. M. Wereley, "Energy harvesting utilizing single crystal PMN-PT material and application to a self-powered accelerometer," *J. Mech. Des.*, vol. 131, no. 9, art. no. 091008, 2009.

[8] S. Roundy and P. K. Wright, "A piezoelectric vibration based generator for wireless electronics," *Smart Mater. Struct.*, vol. 13, no. 5, pp. 1131–1142, 2004.

[9] Y. K. Hong, "Single crystal piezoelectric transducers to harvest vibration energy," *Proc. SPIE*, vol. 6048, art. no. 60480E, 2005.

[10] R. Elfrink, T. M. Kamel, M. Goedbloed, S. Matova, D. Hohlfeld, Y. van Andel, and R. van Schaijk, "Vibration energy harvesting with aluminum nitride-based piezoelectric devices," *J. Micromech. Microeng.*, vol. 19, no. 9, art. no. 094005, 2009.

[11] H. Kim, V. Bedekar, R. A. Islam, W.-H. Lee, D. Leo, and S. Priya, "Laser-machined piezoelectric cantilevers for mechanical energy harvesting," *IEEE Trans. Ultrason. Ferroelectr. Freq. Control*, vol. 55, no. 9, pp. 1900–1905, Sep. 2008.

[12] Y. B. Jeon, R. Sood, J. Jeong, and S. Kim, "MEMS power generator with transverse mode thin film PZT," *Sens. Actuators A*, vol. 122, no. 1, pp. 16–22, Jul. 2005.

[13] H. Liu, C. J. Tay, C. Quan, T. Kobayashi, and C. Lee, "Piezoelectric MEMS energy harvester for low-frequency vibrations with wideband operation range and steadily increased output power," *J. Microelectromech. Syst.*, vol. 20, no. 5, pp. 1131–1142, Oct. 2011.

[14] L. M. Miller, E. Halvorsen, T. Dong, and P. K. Wright, "Modeling and experimental verification of low-frequency MEMS energy harvesting from ambient vibrations," *J. Micromech. Microeng.*, vol. 21, no. 4, art. no. 045029, Apr. 2011.

[15] E. K. Reilly, L. M. Miller, R. Fain, and P. K. Wright, "A study of ambient vibrations for piezoelectric energy conversion," in *9th Int. Workshop on Micro and Nanotechnology for Power Generation and Energy Conversion Applications*, 2009, pp. 312–315.

[16] N. Dutoit, B. Wardle, and S. Kim, "Design considerations for MEMS-scale piezoelectric mechanical vibration energy harvesters," *Integr. Ferroelectr.*, vol. 71, no. 1, pp. 121–160, 2005.

[17] S. Roundy, P. Wright, and J. Rabaey, *Energy Scavenging for Wireless Sensor Networks: With Special Focus on Vibrations*. Boston, MA: Kluwer Academic, 2004.
[18] M. A. Karami and D. J. Inman, "Parametric study of zigzag microstructure for vibrational energy harvesting," *J. Microelectromech. Syst.*, vol. 21, no. 1, pp. 145–160, 2011.
[19] M. A. Karami and D. J. Inman, "Analytical modeling and experimental verification of the vibrations of the zigzag microstructure for energy harvesting," *J. Vib. Acoust.*, vol. 133, no. 1, art. no. 011002, 2011.
[20] M. A. Karami and D. J. Inman, "Electromechanical modeling of the low-frequency zigzag micro-energy harvester," *J. Intell. Mater. Syst. Struct.*, vol. 22, no. 3, pp. 271–282, Feb. 2011.
[21] D. F. Berdy, P. Srisungsitthisunti, X. Xu, J. Rhoads, B. Jung, and D. Peroulis, "Compact low frequency meandered piezoelectric energy harvester," in *9th Int. Workshop on Micro and Nanotechnology for Power Generation and Energy Conversion Applications*, 2009, pp. 71–74.
[22] *IEEE Standard on Piezoelectricity*. ANSI/IEEE Std. 176-1987, 1988.
[23] S. Priya and D. J. Inman, *Energy Harvesting Technologies*. New York, NY: Springer, 2008.
[24] G. Marrocco, A. Fonte, and F. Bardati, "Evolutionary design of miniaturized meander-line antennas for RFID applications," in *IEEE Antennas and Propagation Society Int. Symp.*, 2002, pp. 362–365.
[25] D. Peroulis, S. Pacheco, K. Sarabandi, and L. Katehi, "Electromechanical considerations in developing low-voltage RF MEMS switches," *IEEE Trans. Microw. Theory Tech.*, vol. 51, no. 1, pp. 259–270, 2003.
[26] W. P. Robbins, D. L. Polla, and D. E. Glumac, "High-displacement piezoelectric actuator utilizing a meander-line geometry I. Experimental characterization," *IEEE Trans. Ultrason. Ferroelectr. Freq. Control*, vol. 38, no. 5, pp. 454–460, Jan. 1991.
[27] M. Tani, M. Akamatsu, Y. Yasuda, and H. Toshiyoshi, "A two-axis piezoelectric tilting micromirror with a newly developed PZT-meandering actuator," in *20th IEEE Int. Conf. Micro Electro Mechanical Systems*, 2007, pp. 699–702.
[28] A. Erturk, P. A. Tarazaga, J. R. Farmer, and D. J. Inman, "Effect of strain nodes and electrode configuration on piezoelectric energy harvesting from cantilevered beams," *J. Vib. Acoust.*, vol. 131, no. 1, art. no. 011010, 2009.
[29] S. Roundy, "On the effectiveness of vibration-based energy harvesting," *J. Intell. Mater. Syst. Struct.*, vol. 16, no. 10, pp. 809–823, 2005.
[30] D. F. Berdy, B. Jung, J. F. Rhoads, and D. Peroulis, "Increased-bandwidth, meandering vibration energy harvester," in *Proc. Int. Solid-State Sensors, Actuators, Microsystems Conf.*, 2011, pp. 2638–2641.
[31] N. Dutoit and B. Wardle, "Performance of microfabricated piezoelectric vibration energy harvesters," *Integr. Ferroelectr.*, vol. 83, no. 1, pp. 13–32, Nov. 2006.

David Berdy received his B.S. degree in computer engineering from Rose-Hulman Institute of Technology, Terre Haute, IN, in 2008. He is currently pursuing his Ph.D degree in electrical engineering in the School of Electrical and Computer Engineering at Purdue University, West Lafayette, IN. His research interests include energy harvesting, MEMS transducers, and wireless sensing.

Pornsak Srisungsitthisunti was born in Lampang, Thailand, in 1982. He received his B.S. degree in mechanical engineering from the University of Wisconsin–Madison in 2005. He received his M.S. degree in mechanical engineering from Purdue University, West Lafayette, IN, in 2007, and is currently pursuing his Ph.D degree in the same department. His research interests include ultrafast laser material processing and near-field optics.

Byunghoo Jung received the B.S. degree from Yonsei University, Korea, in 1990, the M.S. degree from KAIST, Korea, in 1992, and the Ph.D. degree from the University of Minnesota–Twin Cities, in 2005. From 1992 to 1999, he was with Samsung Electronics, Korea, where he was involved in the design of video signal driver circuits for flat panel displays. Following receipt of his Ph.D. degree in January 2005, he was with Qualcomm in San Diego as a Senior RF IC Design Engineer until he joined the School of Electrical and Computer Engineering at Purdue University as an Assistant Professor in August 2005. His research interests include analog, RF, and mixed-signal circuit design for wireless and wired communications and bio-medical systems. He is the first place winner of the 2002–2003 SRC SiGe BiCMOS Design Challenge (as a lead designer) and the 2007–2008 SRC/SIA IC Design Challenge (as a lead faculty), and holds 10 US patents. He has been serving as a Co-Chair of the DAC/ISSCC Student Design Contest (SDC) since October 2006, as an Associate Editor of the *IEEE Transactions on Very Large Scale Integration (VLSI) Systems* since January 2009, and as a member of the Analog Signal Processing Technical Program Committee (ASPTPC) in the IEEE Circuits and System Society since May 2006.

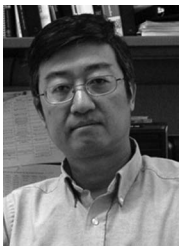

Xianfan Xu is James J. and Carol L. Shuttleworth Professor of Mechanical Engineering at Purdue University. He obtained his M.S. and Ph.D. degrees in mechanical engineering in 1991 and 1994, respectively, both from the University of California, Berkeley. His research interests include developing novel laser processing techniques for laser micro and nano-manufacturing, and fundamental studies of laser-matter interaction and near-field nano-optics. He has given more than 70 invited talks in academic institutes, technical conferences, government laboratories, and industry, and published more than 100 papers in archival journals. He is the recipient of the National Science Foundation Faculty CAREER Award, the Office of Naval Research Young Investigator Award, and the B.F.S. Schaefer Young Faculty Scholar Award of Purdue University. He is a fellow of the American Society of Mechanical Engineers and a Fellow of SPIE.

Jeffrey F. Rhoads is an Assistant Professor in the School of Mechanical Engineering at Purdue University and is affiliated with both the Birck Nanotechnology Center and Ray W. Herrick Laboratories at the same institution. He received his B.S., M.S., and Ph.D. degrees, all in mechanical engineering, from Michigan State University in 2002, 2004, and 2007, respectively. Dr. Rhoads' current research interests include the predictive design, analysis, and implementation of resonant micro/nanoelectromechanical systems (MEMS/NEMS) for use in chemical and biological sensing, signal filtering, and inertial sensing systems, the behavior of nonlinear, parametrically excited systems and coupled oscillators, and the behavior of mechanical and/or electromechanical parametric amplifiers. Dr. Rhoads is a member of the American Society for Engineering Education (ASEE) and the American Society of Mechanical Engineers (ASME), where he serves on both the Student Design Committee and the Design Engineering Division's Technical Committee on Micro/Nanosystems. Dr. Rhoads is a 2009 recipient of the National Science Foundation's Faculty Early Career Development (CAREER) Award and the Purdue School of Mechanical Engineering's Harry L. Solberg Best Teacher Award.

Dimitrios Peroulis received his Ph.D. degree in electrical engineering from the University of Michigan at Ann Arbor in 2003. Since August 2003, he has been with Purdue University, where he is currently leading a group of graduate students on a variety of research projects in the areas of RF MEMS, sensing and power harvesting applications, and RFID sensors for the health monitoring of sensitive equipment. He has been a PI or a co-PI in numerous projects funded by government agencies and industry in these areas. He is currently a key contributor in two DARPA projects at Purdue focusing on 1) very-high-quality ($Q > 1000$) RF tunable filters in mobile form factors (DARPA Analog Spectral Processing Program, Phases I, II, and III) and on 2) developing comprehensive characterization methods and models for understanding the viscoelasticity/creep phenomena in high-power RF MEMS devices (DARPA M/NEMS S&T Fundamentals Program, Phases I and II). Furthermore, he is leading the experimental program on the Center for the Prediction of Reliability, Integrity, and Survivability of Microsystems (PRISM) funded by the National Nuclear Security Administration. In addition, he is heading the development of MEMS technology in a U.S. Navy project (Marines) funded under the Technology Insertion Program for Savings (TIPS) program focused on harsh-environment wireless micro-sensors for the health monitoring of aircraft engines. He has more than 130 refereed journal and conference publications in the areas of microwave integrated circuits, sensors, and antennas. He received the National Science Foundation CAREER award in 2008. His students have received many student paper awards and other student research-based scholarships. He is a Purdue University Faculty Scholar and has also received eight teaching awards, including the 2010 HKN C. Holmes MacDonald Outstanding Teaching Award and the 2010 Charles B. Murphy award, which is Purdue University's highest undergraduate teaching honor.